A near-infrared Counterpart of 2E1613.5–5053: the Central Source in Supernova Remnant RCW103

Tendulkar, S. P.; Kaspi, V. M.; Archibald, R. F.; Scholz, P.

Publisher's version / Version de l'éditeur:
https://doi.org/10.3847/1538-4357/aa6d0c
The Astrophysical Journal, 841, 11, 2017-05-16

The Astrophysical Journal, 841:11 (6pp), 2017 May 20 https://doi.org/10.3847/1538-4357/aa6d0c

A Near-infrared Counterpart of 2E1613.5–5053: The Central Source in Supernova Remnant RCW103

S. P. Tendulkar[1], V. M. Kaspi[1], R. F. Archibald[1], and P. Scholz[2]
[1] Department of Physics and McGill Space Institute, McGill University, 3600 University Street, Montreal QC, H3A 2T8, Canada; shriharsh@physics.mcgill.ca
[2] National Research Council of Canada, Herzberg Astronomy and Astrophysics, Dominion Radio Astrophysical Observatory, P.O. Box 248, Penticton, BC V2A 6J9, Canada
Received 2016 October 7; revised 2017 April 10; accepted 2017 April 10; published 2017 May 16

Abstract

On 2016 June 22, 2E 1613.5−5053, the puzzling central compact object in supernova remnant RCW 103 emitted a magnetar-like burst. Using Director's Discretionary Time, we observed 2E 1613.5−5053 with the *Hubble Space Telescope* (*HST*) (WFC3/IR) and we report here on the detection of a previously unseen infrared counterpart. In observations taken on 2016 July 4 and August 11, we detect a new source ($m_{\rm F110W} = 26.3$ AB mag and $m_{\rm F160W} = 24.2$ AB mag), at the *Chandra* position of 2E 1613.5−5053, that was not detected in *HST*/NICMOS images from 2002 August 15 and October 8, to a depth of 24.5 AB mag (F110W) and 25.5 AB mag (F160W). We show that these deep IR observations rule out the possibility of 2E 1613.5−5053 being an accreting binary with a high degree of confidence, but mimic IR emission properties of magnetars and isolated neutron stars. The presence or absence of a low-mass fallback disk cannot be confirmed from our observations.

Key words: pulsars: individual (2E 1613.1–5053) – stars: neutron

1. Introduction

2E 1613.5−5053 was discovered as a bright X-ray source in the supernova remnant (SNR) RCW 103 using the *Einstein* X-ray Observatory (Tuohy & Garmire 1980). The nature of 2E 1613.5−5053 has been mysterious for the past three decades. With soft thermal X-ray emission, an apparent absence of radio detection, and a location in the center of an SNR, 2E 1613.5−5053 was first classified as a Central Compact Object (CCO; de Luca 2008). However, this classification is fraught with trouble. Unlike CCOs whose X-ray luminosities are usually stable, 2E 1613.5−5053 shows variations in X-ray luminosity over multiple orders of magnitude (Gotthelf et al. 1999; Esposito et al. 2011) on timescales of months and years.

A suprising 6.67 hr periodicity was discovered with nearly 50% modulation in the X-ray band (De Luca et al. 2006) with no hint of faster pulsations. The 6.67 hr periodicity is too slow for the rotation of a young isolated neutron star, requiring exotic explanations for its origin and for braking mechanisms such as wind and/or disk accretion (De Luca et al. 2006; Li 2007). The periodicity is typical of compact binaries and models of tidal locking with a binary companions (Pizzolato et al. 2008), and propeller emission from an accretion disk in a pre-low mass X-ray binary (Bhadkamkar & Ghosh 2009) has been suggested to explain the periodicity as an orbital modulation. However, deep near-infrared (NIR) imaging has limited any binary companion to be less massive than an M6 star, too small to support an accretion luminosity of 10^{34-35} erg s^{-1} (De Luca et al. 2008, hereafter dL08).

On 2016 June 22, the *Swift* Burst Alert Telescope (BAT, Barthelmy et al. 2005) detected a millisecond-timescale magnetar-like burst from the region of SNR RCW 103 (D'Ai et al. 2016). *Swift* slewed its X-ray Telescope (XRT, Burrows et al. 2005) and detected that 2E 1613.5−5053 was in outburst, with an absorbed 0.5–10 keV flux of 4×10^{-11} erg cm^{-2} s^{-1}, substantially higher than the quiescent absorbed flux of 2×10^{-12} erg cm^{-2} s^{-1} in the same band. The short burst, and the double blackbody + hard power-law (spectral index $\Gamma \approx 1.2$) shape of the outburst spectrum suggest the source is a magnetar (D'Aì et al. 2016; Rea et al. 2016), but the origin of the 6.67 hr periodicity remains puzzling. The slowing of a magnetar via magnetic field interactions with a fallback disk was suggested and preferred by many authors but the binary scenario has not been completely ruled out (De Luca et al. 2008; D'Aì et al. 2016; Rea et al. 2016). New theoretical work suggests that a neutron star with a high magnetic field ($B \sim 5 \times 10^{15}$ G) and a fallback disk can efficiently decelerate to rotational periods of a few hours. The estimated mass of the fallback disk required to slow down the disk varies from $10^{-9}\,M_\odot$ (Ho & Andersson 2017) to $10^{-5}\,M_\odot$ (Tong et al. 2016). Whether the fallback disk survives the interaction to the present day is an unanswered question.

1.1. Near-IR Counterpart/Companion

2E 1613.5−5053 lies in the Galactic plane ($l = 332°$, $b = -0°4$) in a crowded stellar field with high extinction. This makes the identification of the counterpart or companion to 2E 1613.5−5053 challenging. Previous authors have attempted identification using photometric variability (Sanwal et al. 2002; Mignani et al. 2008) and also colors in the NIR (dL08). However, no obvious candidate has stood out from the seven candidates in or near the 99% *Chandra* position error ellipse.

The 2016 June 22 outburst provided an opportunity to look for NIR luminosity variations that have been observed during outbursts of magnetars as well as in accretion binaries. Here we describe our Director's Discretionary Time observations with *Hubble Space Telescope* (*HST*)/WFC3 and report a new source that was absent in the 2002 observations.

2. Observations and Analysis

2.1. 2016 Observations

We requested DDT observations of 2E 1613.5−5053 in the F160W (*H* band) and F110W (*Y*+*J* band) filters using the

Table 1
HST Observations of 2E 1613.5−5053

Obs ID	Start–End (UT)	Inst/Filt[a]	Exp[b]
2016 August			
ID4V02VJQ	2016 Aug 11 02:48–02:50	WFC3/F160W	105.5
ID4V02020	2016 Aug 11 02:56–04:16	WFC3/F160W	1287
ID4V02010	2016 Aug 11 02:50–04:10	WFC3/F110W	1287
2016 July			
ID4V01B3Q	2016 Jul 04 02:48–02:50	WFC3/F160W	105.5
ID4V01020	2016 Jul 04 02:56–04:16	WFC3/F160W	1287
ID4V01010	2016 Jul 04 02:50–04:10	WFC3/F110W	1287
2002 October (archival)			
N8C501010	2002 Oct 08 02:26–04:10	NIC2/F160W	2590.5
N8C501020	2002 Oct 08 04:10–06:04	NIC2/F160W	2590.5
N8C501030	2002 Oct 08 06:05–09:09	NIC2/F160W	2590.5
N8C501040	2002 Oct 08 09:10–11:12	NIC2/F160W	2590.5
N8C501050	2002 Oct 08 11:13–12:39	NIC2/F110W	935
2002 August (archival)			
N8C502020	2002 Aug 15 10:28–12:03	NIC2/F160W	2590.5
N8C502040	2002 Aug 15 13:40–14:31	NIC2/F160W	2590.5
N8C502050	2002 Aug 15 15:19–15:41	NIC2/F110W	935
N8C502030	2002 Aug 15 12:04–12:55	NIC2/F160W	2590.5
N8C502010	2002 Aug 15 08:50–10:27	NIC2/F160W	2590.5

Notes.
[a] Instrument and Filter: WFC3—Wide Field Camera 3/IR, NIC2—NICMOS Camera 2.
[b] Exposure time in seconds.

WFC3 instrument. The images were acquired on 2016 July 4 and 2016 August 11, corresponding to 12 and 50 days after the first magnetar-like burst of 2E 1613.5−5053, respectively. The observation details are specified in Table 1. The observations were spaced to detect the likely fading of magnetars over the timescale of a month (see, e.g., Kaspi et al. 2014). However, the average X-ray luminosity of 2E 1613.5−5053 did not decrease significantly over this time period (see Section 2.3).

We used the WFC3/IR camera with a 512 × 512 pixel (68″ × 68″) aperture in both filters. We acquired 4 × 321 s exposures in the F110W band and 1 × 105 s + 4 × 321 s exposures in the F160W band at both epochs. The 321 s exposures in each filter were read out using the `SPARS25` sampling and the 105 s exposure was acquired using the rapid log-linear `STEP25` readout to correctly image bright stars in the field.[3] The exposures were dithered with the standard 4 position dither (`WFC3-IR-DITHER-BOX-MIN`) to improve the sampling of the point-spread function (PSF) and to identify and remove cosmic rays.

We processed the images with the standard `STSDAS` analysis package in `IRAF`. We dedistorted and combined the images to a platescale of 55 mas per pixel in the F160W filter and 37.8 mas per pixel in the F110W filter using the `drizzlepac` package. We chose the platescales to sample the point-spread function (PSF) in each filter with 2.5 pixels.

2.2. 2002 Observations

We downloaded archival NICMOS NIC2 images of 2E 1613.5−5053 acquired in 2002 August and October from the Space Telescope Archive (Program 9467). The details of the data are specified in Table 1. The F110W images from 2002 were shallow (total exposure of 1870s) and only the brightest stars were visible. Hence we only consider the 2002 F110W images to measure upper limits in the analysis. We did not use the F205W (K) band images in this analysis, as they were discussed in dL08.

The image files from the August and October observations were separately dedistorted and combined using `MultiDrizzle` to the same plate scales and settings as the WFC3/IR observations.

2.3. Swift-XRT Observations

As the IR luminosity of magnetars may vary with the X-ray luminosity, we analyzed the 0.5–10 keV X-ray data from *Swift*-XRT observations closest in time to the 2016 *HST* observations. We downloaded the data for observations 00700791011 (2.1 ks exposure at 2016 July 4 13:21 UT) and 00030389037 (2.7 ks exposure at 2016 August 10 01:08 UT) from `HEASARC`, and reduced using the `xrtpipeline` standard reduction script from `HEASOFT v6.17`. To mitigate pile-up effects, we used an annular region with an inner radius of 3 pixels and an outer radius of 20 pixels for extracting the source photons. An annular region with an inner radius of 80 and outer radius of 120 was used for the background.

We fit these spectra with an absorbed blackbody model over 0.5–10.0 keV using `XSPEC 12.9.0n` (Arnaud 1996). Photoelectric absorption was modeled using `XSPEC tbabs` with abundances from Wilms et al. (2000), and photoelectric cross-sections from Verner et al. (1996). The observations were co-fit with a single $N_{\rm H}$, allowing both the blackbody temperature and normalization to vary between observations. The best-fit photoelectric column density was $N_{\rm H} = 1.8^{+0.2}_{-0.3} \times 10^{22}$ cm^{-2}, slightly higher than the $N_{\rm H} = 0.87 \pm 0.35 \times 10^{22}$ cm^{-2} measured by Foight et al. (2016) for the supernova remnant. The small difference is likely due to instrumental calibration differences and different model fitting degeneracies and does

[3] See the instrument handbook for details: http://www.stsci.edu/hst/wfc3.

not affect the results. The measured blackbody temperatures and absorbed fluxes were $kT_1 = 0.63 \pm 0.03$ keV, $kT_2 = 0.58 \pm 0.03$ keV, $F_{X,1} = 2.3^{+0.2}_{-0.3} \times 10^{-11}$ erg cm^{-2} s^{-1}, and $F_{X,2} = 2.4^{+0.1}_{-0.3} \times 10^{-11}$ erg cm^{-2} s^{-1}, where the subscripts 1 and 2 refer to the July and August epochs, respectively. Thus, we conclude that the X-ray flux did not decrease significantly between our *HST* observation epochs, consistent with the slowly decaying X-ray light curve reported by D'Aì et al. (2016) and Rea et al. (2016).

3. Results

3.1. PSF Fitting

For accurate photometry and astrometry, we performed PSF fitting on each image using the `IDL` code `StarFinder` (Diolaiti et al. 2000). We used a 95 × 95 pixel PSF model (5.″2 in F160W and 3.″6 in F110W) to account for the diffraction spikes. We assumed the PSF model to be static over each drizzled image.

For each image, we used fifteen bright stars in the image to create a model PSF that was fit to all the stars in the image. This step was iterated twice and we ensured that the PSF model was cleaned of contaminating stars. We extracted the pixel coordinates and fluxes of stars in each filter and epoch. We limited the search to sources that were detected with a signal to noise ratio (SNR) greater than 3 and where the normalized PSF fitting correlation was greater than 0.8. The residual images were analyzed by eye to verify that no under-fitting or over-fitting had occurred. The PSF model created for each image was saved.

We used the 2016 July F160W image as the reference for matching all objects from other images. We first corrected the world coordinate system of the reference image to the 2MASS star positions (Skrutskie et al. 2006) using the `IRAF` task `ccmap`. The residual fitting error was 0.″11 (root-mean-square). Before fitting, we removed 2MASS sources that corresponded to unresolved stars in the *HST* images. The positions of stars in other images were matched and transformed to the image coordinate system of 2016 July F160W image using the `geomap` and `geoxytran IRAF` tasks. The residuals of the matching were ≈0.4 pix (22 mas). We matched the detected sources using a search radius of 0.5 pixels and produced a combined list of sources and fluxes/non-detections.

3.2. Photometry

The flux reported by `StarFinder` is the integrated flux under the normalized PSF. We converted the flux to AB magnitudes using the `PHOTFNU` keyword based on the WFC3/IR and NICMOS calibration. While `StarFinder` reports a formal flux error for each star, this does not account for the error in PSF estimation, PSF variation over the image and the background estimation. We estimated the scatter in fluxes by comparing the fluxes measured in the 2016 July images to 2016 August images and 2002 August images to the 2002 October images. As the image pairs were acquired with the same instrumental configuration separated only by a few months, the scatter in the fluxes should be dominated by the errors arising from the sources discussed above.

Figure 1 shows the measured magnitudes and magnitude differences in the pairs of images and the calculated scatter in 1 mag bins. The NICMOS F110W images were not used for this analysis, as they did not have sufficient stars to accurately estimate the standard deviation in each magnitude bin. Comparing the photometry between WFC3 and NICMOS, we find that the faint star (>20 mag) photometry matches within errors and there is no significant zero-point difference. The bright star photometry with NICMOS is known to have a nonlinearity[4] and it is detectable at a 0.1 mag level for bright stars.

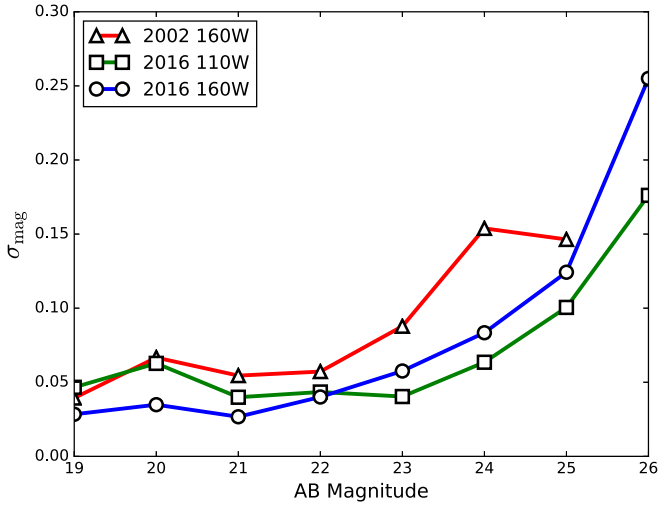

Figure 1. 1σ scatter in photometry for the 2016 WFC3 F110W (squares), F160W (circles), and 2002 NICMOS F160W images (triangles). The scatter is due to a combination of PSF modeling errors, PSF variation over the image, background contribution, and the Poisson noise. The 2002 NICMOS F110W images did not have sufficiently many stars to accurately estimate the standard deviation in each magnitude bin.

3.3. Detected Sources

We labeled the sources detected in the field following the scheme used in dL08 (Figure 2). We detected a new object, Source 8, in the 2016 images inside the *Chandra* position ellipse. The magnitudes of the source, along with photometric scatter (as calculated above), are given in Table 2.

Source 8 was not detected in the 2002 images (Figure 3, left panel). As a verification, we converted the measured F160W flux from the 2016 July measurement into the expected NICMOS count rate. Using the PSF extracted from the 2002 August and 2002 October images, we injected a fake source at the location of source 8. The source is clearly visible and also detected by the same analysis pipeline as utilized above (Figure 3, middle panel). By reducing the brightness of the injected source until it was not detected in our analysis pipeline, we estimate the limiting brightness of source 8 in 2002 August and 2002 October (Table 2). We put 3σ upper limits of $m_{\rm F110W} > 24.5$ and $m_{\rm F160W} > 25.2$ for individual images. If the 2002 August and October images are combined, the limiting magnitudes are $m_{\rm F110W} \gtrsim 25$ and $m_{\rm F160W} \gtrsim 25.5$.

4. Discussion

Following the 2016 magnetar flare and X-ray brightening of 2E 1613.5−5053, we have detected a new infrared source at the X-ray location of 2E 1613.5−5053. The infrared source brightened by at least 1.3 mag (F160W) compared to the non-

[4] http://www.stsci.edu/hst/nicmos/performance/anomalies/nonlinearity.html

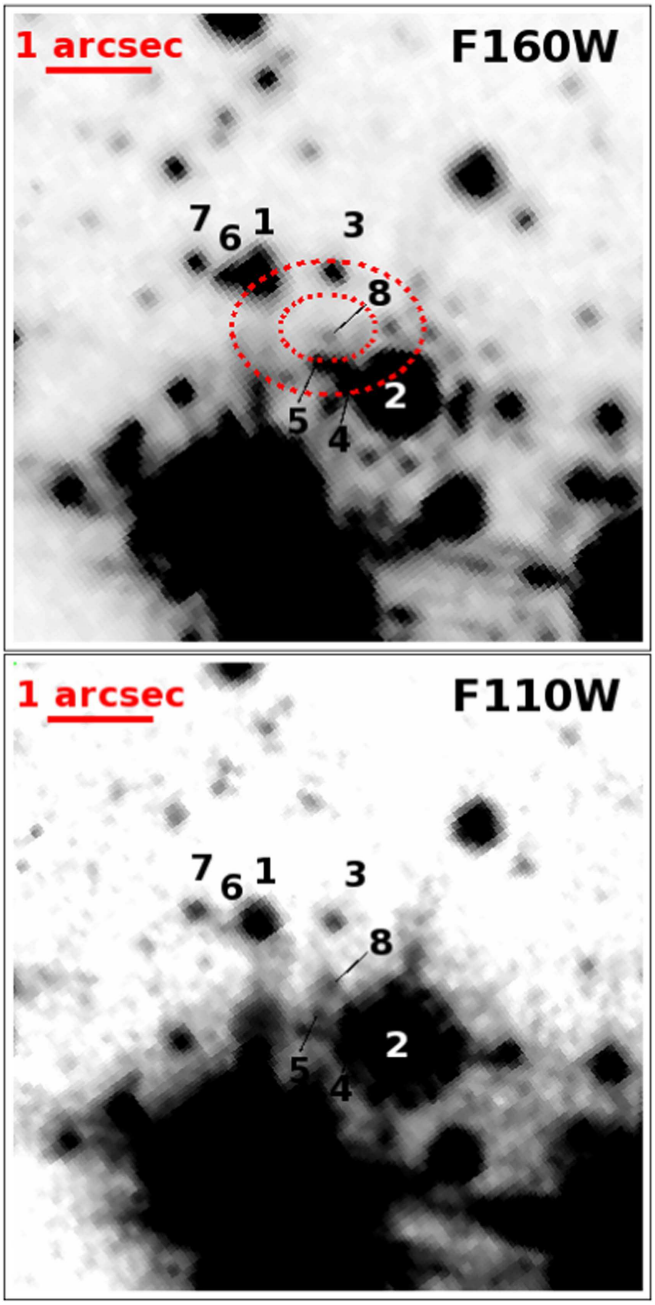

Figure 2. WFC3 F160W (top panel) and F110W (bottom panel) images of 2E 1613.5−5053 from 2016 July. The stars are labeled following dL08 and the new detection, source 8, is marked. The dotted ellipse shows the 68% and 99% position error ellipses calculated by dL08.

detections in previous 2002 observations. Thus, we conclude that this source is associated with 2E 1613.5−5053 and we discuss the implications and the physical scenarios for explaining its 6.67 hr X-ray modulation.

Roche Lobe Radius—Assuming the 6.67 hr period as the orbital period of a 1.4 $M_\odot$ neutron star binary, we calculated the relation between the companion mass and Roche radius (Eggleton 1983). Using a mass–radius relation for main-sequence stars[5] (Pecaut & Mamajek 2013), we find that main-sequence stars less massive than 0.8 $M_\odot$ (corresponding to temperatures lower than 5000 K, spectral type K2V) are smaller than the Roche lobe radius and would not undergo accretion in such a system. We can also rule out accretion from white dwarfs, as their radii are very small—the Roche radius for a 0.2 $M_\odot$ companion (a low mass white dwarf) is 0.5 $R_\odot$ and increases with companion mass.

Dust Extinction in IR—To interpret the nature of the source, we must first try to determine its intrinsic brightness, corrected for extinction. The magnitude of the optical/IR extinction toward 2E 1613.5−5053 is uncertain. The dust maps of Schlafly & Finkbeiner (2011) estimate $A_V = 36$ mag in the direction of 2E 1613.5−5053.[6] This is also supported by the average $H - K$ color of the surrounding stars from dL08 who estimate $A_V = 20$–40 for the whole field. However, the near-IR spectroscopy of RCW 103 (Oliva et al. 1989) and the photoelectric absorption column density ($N_{\rm H}$) estimated from X-ray observations of 2E 1613.5−5053 and RCW 103 (Foight et al. 2016) suggest a much lower value of $A_V = 3$–6. Considering the $N_{\rm H} = 2.87 \pm 0.12 \times 10^{21} A_V$ cm^{-2} relation (Güver & Özel 2009; Foight et al. 2016), an $A_V = 20$–40 would require a column density of $\approx$5–10 $\times$ 10^{22} cm^{-2}, far greater than the Galactic hydrogen column density ($N_{\rm HI} \approx 2 \times 10^{22}$ cm^{-2}) for the entire Galaxy along that line of sight (Kalberla et al. 2005; McClure-Griffiths et al. 2009).

Here, we discuss both the high extinction case ($A_V = 36$ mag) and the low extinction case ($A_V = 3.6$ mag) assuming a distance of 3.3 kpc to RCW 103 (Tuohy & Garmire 1980), but considering that the low extinction value is substantially more likely since it arises from measurements of 2E 1613.5−5053 and RCW 103 themselves. We also show that the high extinction case leads to infeasible scenarios.

For each case, we discuss whether the IR emission could be due to a companion/accretion disk (binary scenario), in which case the 6.67 hr period could be interpreted as the orbital period. We also discuss, alternatively, whether the IR emission is from the neutron star or a fallback disk (isolated scenario), where the 6.67 hr period is interpreted as the rotational period of the neutron star.

The 0.5–10 keV X-ray flux at the 2002 and 2016 observation epochs was approximately 6 $\times$ 10^{-12} erg cm^{-2} s^{-1} dL08 and 4.5 $\times$ 10^{-11} erg cm^{-2} s^{-1} (Rea et al. 2016), respectively. This corresponds to intrinsic luminosities of $L_{\rm X} = 7 \times 10^{33}$ erg s^{-1} and $L_{\rm X} = 5 \times 10^{34}$ erg s^{-1}, an increase by a factor of $\sim$7.

4.1. High Extinction Case

If $A_V = 36$ mag, the extinctions in the F110W and F160W bands are 9.5 mag and 6.0 mag, respectively. Thus, including a distance modulus of $5\log(3.3\ {\rm kpc}/10\ {\rm pc}) = 12.6$ mag, the absolute AB magnitudes of source 8 in 2016 are 4.2 (F110W) and 5.6 (F160W). The corresponding limits in 2002 are >2.4, and >6.9 AB mag, respectively.

We compared the absolute magnitudes to stellar spectro-photometry (Pecaut & Mamajek 2013) and white dwarf models (Bergeron et al. 2011; Tremblay et al. 2011, and references therein[7]). The 2002 NICMOS upper limits are consistent with main-sequence stars cooler than M2V (corresponding to masses <0.5 $M_\odot$) or with DA and DB white dwarfs as companions to 2E 1613.5−5053. The magnitude limits also rule out all giant and supergiant stars (luminosity classes I-IV). dL08 also used

[5] See http://www.pas.rochester.edu/~emamajek/EEM_dwarf_UBVIJHK_colors_Teff.txt.

[6] http://irsa.ipac.caltech.edu/applications/DUST/.

[7] See http://www.astro.umontreal.ca/~bergeron/CoolingModels/.

Table 2
Photometry of Sources near the Location of 2E 1613.5−5053

	2002				2016			
	Aug		Oct		Jul		Aug	
#	$m_{\rm F110W}$	$m_{\rm F160W}$	$m_{\rm F110W}$	$m_{\rm F160W}$	$m_{\rm F110W}$	$m_{\rm F160W}$	$m_{\rm F110W}$	$m_{\rm F160W}$
1	23.8 ± 0.2	21.20 ± 0.06	23.8 ± 0.2	21.16 ± 0.06	23.84 ± 0.07	21.44 ± 0.04	23.76 ± 0.07	21.40 ± 0.04
2[a]	19.1 ± 0.1	18.02 ± 0.04	19.1 ± 0.1	18.01 ± 0.04	19.70 ± 0.06	18.37 ± 0.03	19.63 ± 0.06	18.38 ± 0.03
3	>24.5	22.92 ± 0.09	>24.5	22.91 ± 0.09	25.55 ± 0.15	23.04 ± 0.06	25.45 ± 0.15	23.05 ± 0.06
4	>24.5	22.50 ± 0.08	>24.5	22.61 ± 0.08	25.53 ± 0.14	22.90 ± 0.06	25.65 ± 0.15	23.04 ± 0.06
5	>24.5	23.19 ± 0.11	>24.5	23.20 ± 0.11	26.51 ± 0.21	23.53 ± 0.07	26.19 ± 0.20	23.51 ± 0.07
6	>24.5	23.25 ± 0.11	>24.5	23.20 ± 0.11	26.45 ± 0.21	23.50 ± 0.07	26.26 ± 0.20	23.46 ± 0.07
7	>24.5	22.96 ± 0.09	>24.5	22.94 ± 0.09	25.37 ± 0.12	23.11 ± 0.06	25.26 ± 0.12	23.09 ± 0.06
8[b]	>24.5	>25.2	>24.5	>25.2	26.27 ± 0.20	24.24 ± 0.08	26.39 ± 0.21	24.51 ± 0.10

Notes. All magnitudes are measured in the AB magnitude scale.
[a] Star 2 is affected by the photometric nonlinearity of the NICMOS detector and hence the difference in 2002 and 2016 magnitudes is not astrophysical.
[b] New source detected only in 2016 observations.

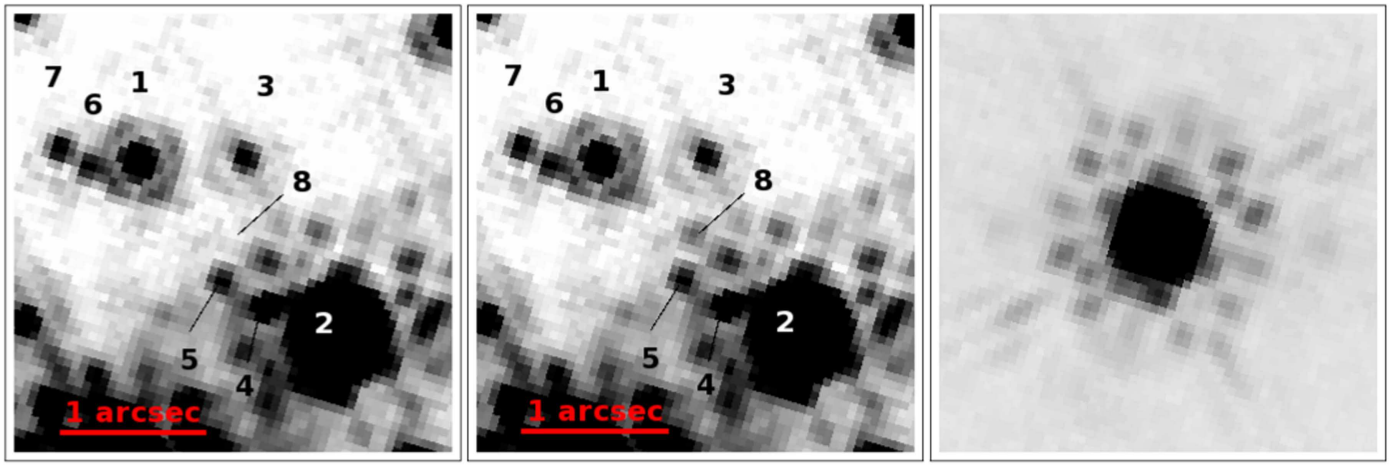

Figure 3. Verifying the detectability of source 8 in 2002 F160W images. Left panel: original 02-J-160 image. Middle panel: 02-J-160 image with source 8 injected by scaling the extracted PSF (right panel) to an AB magnitude of 24.2 mag. The source is easily detected. The bright spots to the lower right of source 8 in the middle panel are speckles of the PSF as shown in the right panel.

deeper K_s band VLT upper limits to rule out any binary companions brighter than a M6-M8 dwarf.

In this case, the accreting binary scenario is ruled out for the following reasons. First, as discussed above, main-sequence stars less massive than K2V, and all white dwarfs, are too small for Roche lobe overflow. Second, the calculated intrinsic F110W−F160W color of −1.4 mag in the 2016 observations is bluer than blackbodies of 10^{15} K, ruling out any interpretation of the infrared flux as blackbody emission from a star or an accretion disk. Interpreting the color as power-law emission (ν^{α}), we get $\alpha \approx 4.5$, rising far steeply than the observed spectra from low-mass X-ray binary accretion disks ($0.5 \lesssim \alpha \lesssim 1.5$) (Hynes 2005).

In this high extinction case, the 2016 IR luminosity of 2E 1613.5−5053 corresponds to $L_{\rm F110W} = 10^{33}$ erg s^{-1} and $L_{\rm F160W} = 2 \times 10^{32}$ erg s^{-1}. Comparing the IR and X-ray luminosities, we get $L_{\rm X}/L_{\rm F110W,F160W} \approx 50$–$200$. This ratio of X-ray to IR luminosities is also significantly lower than the values of 10^4 observed for isolated neutron stars, magnetars, and CCOs (Fesen et al. 2006; Wang et al. 2006; Mignani et al. 2008).

Thus, we find that the high extinction scenario leads to astrophysically infeasible cases and we do not discuss it further.

4.2. Low Extinction Case

If $A_V = 3.6$, the extinctions in the F110W and F160W bands are 0.9 mag and 0.6 mag, respectively. This leads to absolute AB magnitudes in 2016 of 12.8 (F110W) and 11.0 (F160W). The corresponding 2002 upper limits are >11.0 AB mag and >12.3 AB mag, respectively.

For a companion object, the 2002 F110W limit is inconsistent with stars hotter than M7 ($T > 2650$ K) and the F160W limits are inconsistent with stars hotter than L4-L5 ($T > 1600$–1700 K) (Pecaut & Mamajek 2013) and thus cannot contribute to a Roche lobe overflow.

The F110W and F160W luminosities are $L_{\rm F110W} = 4 \times 10^{29}$ erg s^{-1} and $L_{\rm F160W} = 7 \times 10^{29}$ erg s^{-1}. The corresponding X-ray to IR fluence ratios $L_{\rm X}/L_{\rm F110W,F160W} \approx 10^5$ are consistent with those of magnetars such as 4U 0142+61 (Hulleman et al. 2004), 1E 1048.1−5937 (Tam et al. 2008), and limits on other magnetars (Fesen et al. 2006; Wang et al. 2006; Mignani et al. 2008). It is not clear, however, whether this emission arises from the magnetosphere of the neutron star or whether it arises from a fallback disk, as has been suggested around 4U 0142+61 (Wang et al. 2006) and 1E 2259+586 (Kaplan et al. 2009). Wang et al. (2007) measured *Spitzer* flux upper limits to be 10^{-4} Jy (4.5 μm)

and 3×10^{-4} Jy (8 μm). These measurements do not rule out the presence of a disk as massive as the one around 4U 0142 +61 ($10\,M_{\oplus} = 6 \times 10^{28}$ g). Indeed, the amount of material required to slow down the magnetar to its current period is tiny —Ho & Andersson (2017) estimate it to be 10^{24} g, while Tong et al. (2016) estimate the mass to be 10^{28} g.

Intermediate Values of Extinction—If the extinction values are intermediate between the cases considered above, the accretion scenario is still ruled out since it only changes the companion spectral type limit between the M2V and L4V set by the high and low extinction case—still inconsistent with the Roche lobe accretion. However, a different value of extinction will change the $L_X/L_{F110W,F160W}$ ratio. This ratio could vary by a factor of 10 or so and would still be consistent with the wide range of $L_X/L_{F110W,F160W}$ ratios for magnetars and isolated neutron stars discussed above.

Thus, while the presence or absence of a fallback disk cannot be confirmed at this point, we have shown that the binary scenarios for the evolution of 2E 1613.5−5053 can be ruled out with a high level of confidence. Further understanding of the nature of 2E 1613.5−5053 can be achieved via spectroscopy of the faint IR source to search for disk emission features and whether the continuum is better described by a power-law spectrum or a disk blackbody spectrum. While this is extremely challenging with current observational capabilities, it may be possible with the *James Webb Space Telescope*.

The authors thank the *Hubble Space Telescope* operations teams for their speed and flexibility scheduling these observations.

This work is based on observations made with the NASA/ESA *HST*, obtained from the Data Archive at the Space Telescope Science Institute, which is operated by the Association of Universities for Research in Astronomy, Inc., under NASA contract NAS 5-26555. These observations are associated with programs #9467 and #14814. This work also made use of data supplied by the UK Swift Science Data Centre at the University of Leicester.

S.P.T. acknowledges support from a McGill Astrophysics postdoctoral fellowship. V.M.K. receives support from an NSERC Discovery Grant, an Accelerator Supplement, and from the Gerhard Herzberg Award, an R. Howard Webster Foundation Fellowship from the Canadian Institute for Advanced Study, the Canada Research Chairs Program, and the Lorne Trottier Chair in Astrophysics and Cosmology. R.F.A. acknowledges support from an NSERC CGSD. P.S. received support from a Schulich Graduate Fellowship from McGill University and holds a Covington Fellowship at DRAO.

Facilities: *HST* (WFC3/IR, NICMOS) *Swift* (XRT). *Software:* IRAF, StarFinder (Diolaiti et al. 2000).

References

Arnaud, K. A. 1996, in ASP Conf. Ser. 101, Astronomical Data Analysis Software and Systems V, ed. G. H. Jacoby & J. Barnes (San Francisco, CA: ASP), 17
Barthelmy, S. D., Barbier, L. M., Cummings, J. R., et al. 2005, SSRv, 120, 143
Bergeron, P., Wesemael, F., Dufour, P., et al. 2011, ApJ, 737, 28
Bhadkamkar, H., & Ghosh, P. 2009, A&A, 506, 1297
Burrows, D. N., Hill, J. E., Nousek, J. A., et al. 2005, SSRv, 120, 165
D'Aì, A., Evans, P. A., Burrows, D. N., et al. 2016, MNRAS, 463, 2394
D'Ai, A., Evans, P. A., Gehrels, N., et al. 2016, ATel, 9180
de Luca, A. 2008, in AIP Conf. Ser. 983, 40 Years of Pulsars: Millisecond Pulsars, Magnetars and More, ed. C. Bassa et al. (Melville, NY: AIP), 311
De Luca, A., Caraveo, P. A., Mereghetti, S., Tiengo, A., & Bignami, G. F. 2006, Sci, 313, 814
De Luca, A., Mignani, R. P., Zaggia, S., et al. 2008, ApJ, 682, 1185
Diolaiti, E., Bendinelli, O., Bonaccini, D., et al. 2000, A&AS, 147, 335
Eggleton, P. P. 1983, ApJ, 268, 368
Esposito, P., Turolla, R., de Luca, A., et al. 2011, MNRAS, 418, 170
Fesen, R. A., Pavlov, G. G., & Sanwal, D. 2006, ApJ, 636, 848
Foight, D. R., Güver, T., Özel, F., & Slane, P. O. 2016, ApJ, 826, 66
Gotthelf, E. V., Petre, R., & Vasisht, G. 1999, ApJL, 514, L107
Güver, T., & Özel, F. 2009, MNRAS, 400, 2050
Ho, W. C. G., & Andersson, N. 2017, MNRAS, 464, L65
Hulleman, F., van Kerkwijk, M. H., & Kulkarni, S. R. 2004, A&A, 416, 1037
Hynes, R. I. 2005, ApJ, 623, 1026
Kalberla, P. M. W., Burton, W. B., Hartmann, D., et al. 2005, A&A, 440, 775
Kaplan, D. L., Chakrabarty, D., Wang, Z., & Wachter, S. 2009, ApJ, 700, 149
Kaspi, V. M., Archibald, R. F., Bhalerao, V., et al. 2014, ApJ, 786, 84
Li, X.-D. 2007, ApJL, 666, L81
McClure-Griffiths, N. M., Pisano, D. J., Calabretta, M. R., et al. 2009, ApJS, 181, 398
Mignani, R. P., Zaggia, S., Dobrzycka, D., et al. 2008, in AIP Conf. Ser. 983, 40 Years of Pulsars: Millisecond Pulsars, Magnetars and More, ed. C. Bassa et al. (Melville, NY: AIP), 325
Oliva, E., Moorwood, A. F. M., & Danziger, I. J. 1989, A&A, 214, 307
Pecaut, M. J., & Mamajek, E. E. 2013, ApJS, 208, 9
Pizzolato, F., Colpi, M., De Luca, A., Mereghetti, S., & Tiengo, A. 2008, ApJ, 681, 530
Rea, N., Borghese, A., Esposito, P., et al. 2016, ApJ, 828, 13
Sanwal, D., Garmire, G. P., Garmire, A., Pavlov, G. G., & Mignani, R. 2002, BAAS, 34, 764
Schlafly, E. F., & Finkbeiner, D. P. 2011, ApJ, 737, 103
Skrutskie, M. F., Cutri, R. M., Stiening, R., et al. 2006, AJ, 131, 1163
Tam, C. R., Gavriil, F. P., Dib, R., et al. 2008, ApJ, 677, 503
Tong, H., Wang, W., Liu, X. W., & Xu, R. X. 2016, ApJ, 833, 265
Tremblay, P.-E., Bergeron, P., & Gianninas, A. 2011, ApJ, 730, 128
Tuohy, I., & Garmire, G. 1980, ApJL, 239, L107
Verner, D. A., Ferland, G. J., Korista, K. T., & Yakovlev, D. G. 1996, ApJ, 465, 487
Wang, Z., Chakrabarty, D., & Kaplan, D. L. 2006, Natur, 440, 772
Wang, Z., Kaplan, D. L., & Chakrabarty, D. 2007, ApJ, 655, 261
Wilms, J., Allen, A., & McCray, R. 2000, ApJ, 542, 914